

## Formation of a Hydrogen Atom from the Photodissociation of Hydrogen Peroxide at 193 nm<sup>#</sup>

Yousuke INAGAKI, Yutaka MATSUMI, and Masahiro KAWASAKI\*

Institute for Electronic Science and Graduate School of Environmental Earth Science, Hokkaido University, Sapporo 060

(Received April 16, 1993)

Doppler profiles of H atoms from the photodissociation of H<sub>2</sub>O<sub>2</sub> at 193 nm were measured by a laser-induced fluorescence method at 121.6 nm. On the average, 149 kJ mol<sup>-1</sup> of energy is released as translational energy, which corresponds to about 60% of the available energy. Doppler width anisotropy data show that the anisotropy parameter,  $\beta$ , for the photofragment angular distribution is  $-0.26 \pm 0.11$ . This result implies that the H<sub>2</sub>O<sub>2</sub>  $\tilde{A}^1A$  state is responsible for H atom formation.

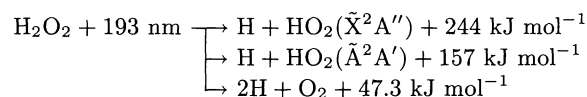
The electronic absorption spectra of H<sub>2</sub>O<sub>2</sub> have been studied both theoretically and experimentally in the ultraviolet and vacuum ultraviolet regions. The promotion of an electron to repulsive sigma orbitals induces a dissociation of H<sub>2</sub>O<sub>2</sub>.<sup>1,2)</sup> The first absorption band extends towards long wavelengths. At 350 nm the cross section is  $10^{-24}$  cm<sup>2</sup> and at 180 nm, it is  $1.4 \times 10^{-18}$  cm<sup>2</sup>, the maximum.<sup>3)</sup> The vertical excitation energies at the equilibrium geometry were calculated by Morita and Kato<sup>2)</sup> to be 576 kJ mol<sup>-1</sup> (193 nm) for the  $\tilde{A}^1A$  state and 724 kJ mol<sup>-1</sup> (165 nm) for the  $\tilde{B}^1B$  state. Since the potential energy surfaces of the excited states are strongly repulsive, it is supposed that the absorption band is very wide toward long wavelengths. Excitation in the long-wavelength tail of the absorption is likely to involve hot-band excitation, primarily the  $\nu_4$  torsional mode: about 10% of the ground-state population is in  $\nu_4=1$  at 300 K. Actually, photodissociation at 248 and 266 nm has been reported to occur after exclusive photoexcitation to the  $\tilde{A}^1A$  state.<sup>4)</sup> The dynamics of the dissociation of H<sub>2</sub>O<sub>2</sub> to OH+OH have been extensively investigated by measuring the rotational and vibrational distribution of the OH fragment as well as via theoretical calculations concerning the electronically excited dissociative states.<sup>1,2)</sup> The  $\tilde{A}^1A \leftarrow \tilde{X}^1A$  transition essentially has a dipole moment along the  $C_2$  symmetry axis. On the other hand, the  $\tilde{B}^1B \leftarrow \tilde{X}^1A$  transition comprises an orbital transition which is essentially aligned parallel to the O–O internuclear axis and leads mainly to a rupture of the O–O bond.

Figure 1 gives a schematic of the potential energy surfaces of the low-lying electronic states of H<sub>2</sub>O<sub>2</sub> as a function of the bond distances,  $R$ , and the torsional angle,  $\tau$ , between the two H–O–O planes after Morita and Kato.<sup>2)</sup> The potential surface of the ground state near to the equilibrium configuration is very flat over  $\tau$ : one can see that the Franck–Condon region is fairly wide along  $\tau$ , considering the zero-point vibration and the thermal distribution. It is apparent from Fig. 1 that the potential curves of both  $\tilde{A}^1A$  and  $\tilde{B}^1B$ , the states reached after UV light absorption, have a torsional dependence much more prominent than that of the  $\tilde{X}$  state.<sup>2)</sup> Re-

moval of an electron from the 4b (n) lone-pair orbital reduces lone-pair repulsion, thus increasing the torsion angle; it is a source of rotational excitation of the OH photofragment.<sup>9)</sup>

The  $\tilde{A} \leftarrow \tilde{X}$  and  $\tilde{B} \leftarrow \tilde{X}$  transitions are complex mixture of valence and Rydberg transitions mixed into the higher Rydberg natures to such an extent that there is no final level that can be called, simply  $\sigma^*$ .<sup>5)</sup> When OH\* antibonding orbitals in H<sub>2</sub>O<sub>2</sub> are excited, hydrogen atoms are produced as photofragments. Thus, at the shorter vacuum UV region the quantum yield of H atom formation increases. Gerlach–Meyer et al.,<sup>6)</sup> Vaghjiani et al.<sup>7)</sup> as well as Stief and De Carlo<sup>8)</sup> have reported on the quantum yield of H atom formation:  $\Phi(H)=0$  at 248 nm,  $0.024 \pm 0.012$  at 222 nm,  $0.16 \pm 0.04$  or  $0.12 \pm 0.01$  at 193 nm, and ca. 0.5 at 123.6 nm.

Hydrogen atom production at 193 nm can occur via three different primary processes:



From measurements of the kinetic energy and angular distribution of an H atom, we could assign a dominant dissociation process and an electronic transition responsible for H atom formation.

### Experimental

Doppler profiles of the H atoms were measured with a laser-induced-fluorescence (LIF) method at the Lyman- $\alpha$  wavelength. The probe light for H and D atoms around 121.6 nm was generated by four-wave mixing using a  $2\omega_1-\omega_2$  scheme in a Kr gas cell (1.3 kPa) with two tunable dye lasers pumped by a XeCl excimer laser (308 nm, 200 mJ/pulse).<sup>10)</sup> The output of the vacuum UV light passing through the reaction cell was monitored by a vacuum UV monochromator and a solar-blind photomultiplier. The laser-induced fluorescence was observed by another solar-blind photomultiplier at right angles to both the photolysis and probe lasers through a LiF window and a band-pass filter (Acton Research, Model 122-VN,  $\lambda=122$  nm,  $\Delta\lambda=12$  nm). The delay between the photolysis and probe light pulses was 100 ns, which was controlled with a time jitter of about 10 ns. An ArF excimer laser (Lambda Physik, EMG 101) was used as a light source at 193 nm. The laser light was polarized by a pile-of-plate

<sup>#</sup>This paper is dedicated to the late Professor Hiroshi Kato.

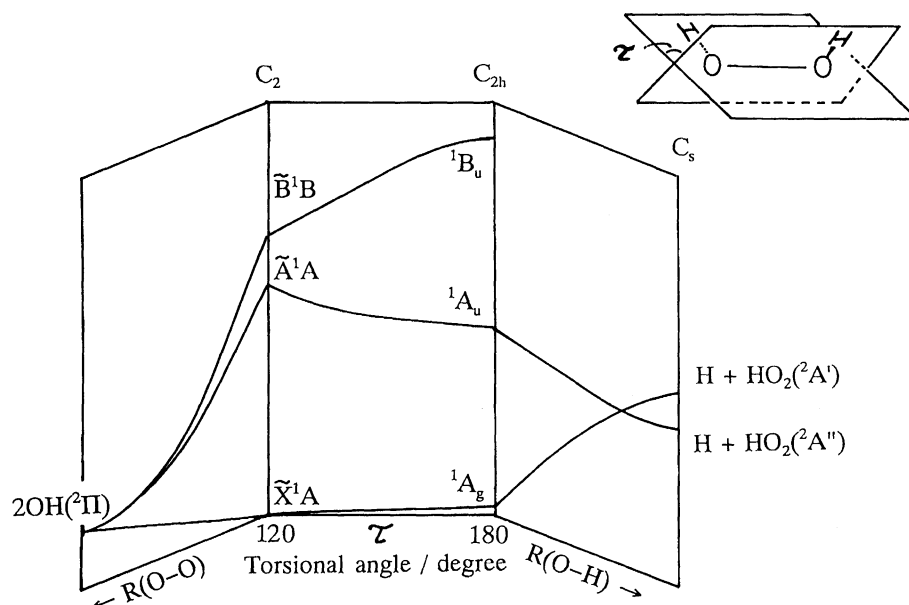


Fig. 1. Potential energy contours and correlations for the low-lying singlet electronic states of  $\text{H}_2\text{O}_2$ , showing the dependence upon the torsional angle,  $\tau$ , after Morita and Kato (Ref. 2).

polarizer. The  $60 \times 60 \times 60$  mm cell was pumped by a rotary pump with a liq.  $\text{N}_2$  trap.

For measuring the polarization effect on the Doppler profiles, two linearly polarized laser beams were perpendicularly crossed with each other. Two different polarization configurations,  $\mathbf{E}_d // \mathbf{k}_p$  and  $\mathbf{E}_d \perp \mathbf{k}_p$ , were used, where  $\mathbf{E}_d$  is the polarization vector of the dissociation laser and  $\mathbf{k}_p$  is the propagation direction of the probe laser. Since the beam diameter of the photolysis laser was sufficiently large (2 mm), within a 100 ns delay the reactions were presumed to proceed homogeneously in the probing region, thus allowing the escape of products from the viewing zone to be ignored. This was tested by Doppler measurements of H atoms from HCl photodissociation at 157 nm, which reproduced the expected value of the translational energy ( $323 \text{ kJ mol}^{-1}$ ).

### Results

Figure 2 shows the Doppler profiles of the H atoms from the photodissociation of  $\text{H}_2\text{O}_2$  at 193 nm by the LIF technique. By scanning the laser wavelength around the resonance frequency of the hydrogen atom at 121.6 nm, the shape of the fluorescence excitation curve was measured. These Doppler widths are much larger than the laser line width ( $0.4 \text{ cm}^{-1}$ ). For measurements of the polarization effect on the Doppler profiles, two linearly polarized laser beams were perpendicularly crossed with each other. Two different polarization configurations of  $\mathbf{E}_d // \mathbf{k}_p$  and  $\mathbf{E}_d \perp \mathbf{k}_p$  were used.

The velocity distribution of atoms from the photodissociation of a molecule is generally given by

$$f(\mathbf{v}) \propto 1 + \beta P_2(\boldsymbol{\varepsilon} \cdot \mathbf{v}), \quad (1)$$

where  $\beta$  is the anisotropy parameter,  $P_2(x)$  the second-Legendre polynomial, and  $\boldsymbol{\varepsilon}$  the electric vector of incident photons. This leads to the following spectral

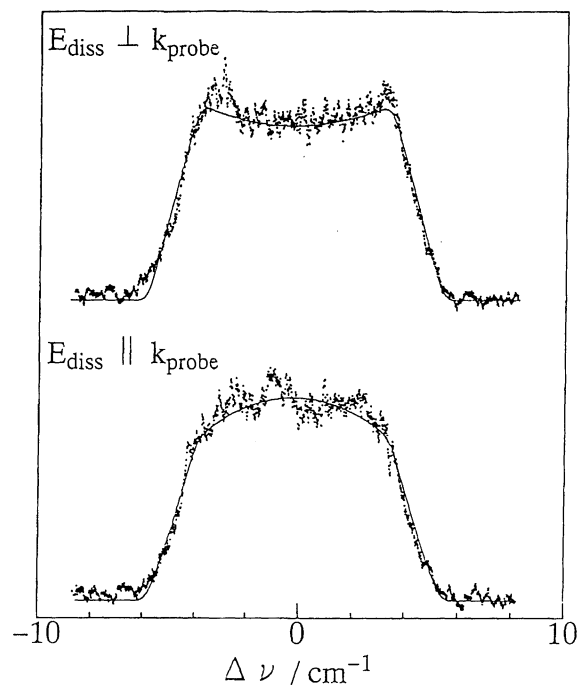


Fig. 2. Vacuum ultraviolet laser induced fluorescence spectra of photofragment H atoms from the photodissociation of  $\text{H}_2\text{O}_2$  at 193 nm.  $\mathbf{E}_{\text{diss}}$  and  $\mathbf{k}_{\text{probe}}$  are the electric vectors of the dissociation laser light and the direction of propagation of the probe laser light, respectively. The solid curves are simulated to those of Eq. 5, using an anisotropy parameter of  $\beta_{\text{eff}} = -0.23$ , an H atom translational energy of  $145 \text{ kJ mol}^{-1}$  and an energy width of  $38 \text{ kJ mol}^{-1}$ .

profile of a photofragment atom,

$$g(\nu) \propto 1 + b\beta P_2\left(\frac{v_z}{v}\right)\Theta(v - |v_z|),$$

where

$$v_z = (\nu - \nu_0)c/\nu_0 \quad (2)$$

Here,  $c$  is the speed of light,  $\Theta(x)$  is the step function,  $\nu$  is the frequency of the probe laser light, and  $\nu_0$  is the resonance center wavenumber of H or D atoms. The value of  $b$  in Eq. 2 is 1 for the perpendicular configuration of the dissociation and probe laser beams.<sup>11)</sup>

The effective anisotropy parameter,  $\beta_{\text{eff}}$ , for the angular distributions of the photofragments are calculated by

$$\beta_{\text{eff}} = 5\{ \langle v_{\parallel}^2 \rangle - \langle v_{\perp}^2 \rangle \} / \{ \langle v_{\parallel}^2 \rangle + 2\langle v_{\perp}^2 \rangle \}, \quad (3)$$

where  $\langle v_{\parallel}^2 \rangle$  and  $\langle v_{\perp}^2 \rangle$  are the average of the squared velocity projection parallel and perpendicular to the polarization vector of the photolysis laser, respectively.<sup>12)</sup> The values of  $\langle v_{\parallel}^2 \rangle$  and  $\langle v_{\perp}^2 \rangle$  can be derived from the second moments of the Doppler profiles at the  $\theta=0^\circ$  and  $90^\circ$  configurations, where  $\theta$  is the angle between the electric vectors of the linearly polarized dissociation laser ( $\mathbf{E}_d$ ) and the propagation direction of the probe laser ( $\mathbf{k}_p$ ). The effective anisotropy parameter thus calculated is  $-0.23 \pm 0.10$ .

The average translational energy of the H fragment in the laboratory frame was  $145 \text{ kJ mol}^{-1}$  by the following equation:

$$\langle E_{\text{t}}^{\text{lab}}(\text{H}) \rangle = (1/2)m_{\text{H}}\{ \langle v_{\parallel}^2 \rangle + 2\langle v_{\perp}^2 \rangle \}. \quad (4)$$

The average total translational energy  $\langle E_{\text{t}}(\text{H} + \text{HO}_2) \rangle$  in the center-of-mass-frame was calculated to be  $149 \text{ kJ mol}^{-1}$ .

Three channels can be considered for the H atom formation from  $\text{H}_2\text{O}_2$  at 193 nm,  $\text{H} + \text{HO}_2(\tilde{\text{X}})$ ,  $\text{H} + \text{HO}_2(\tilde{\text{A}})$ , and  $2\text{H} + \text{O}_2$ , which have excess energies 244, 157, and  $47.3 \text{ kJ mol}^{-1}$ , respectively. Our Doppler spectroscopy for the H atoms implies that the  $\text{H} + \text{HO}_2(\tilde{\text{X}})$  channel is the major one of the three channels, since a counter fragment is usually excited in its ro-vibrational mode, and, thus, the translational energy of the fragments cannot reach the maximum available energy.

Using the anisotropy parameter and translational energy,  $\langle E_{\text{t}}^{\text{lab}}(\text{H}) \rangle$ , the Doppler profiles are simulated by the solid curves of Fig. 2, using the following formula:

$$g(v, \nu) = \frac{1}{2v\nu_0} \left[ 1 + \beta_{\text{eff}} P_2(\cos \chi) P_2\left(\frac{c}{v} \cdot \frac{\nu - \nu_0}{\nu_0}\right) \right],$$

$$\text{for } \frac{c}{v} \left| \frac{\nu - \nu_0}{\nu_0} \right| < 1, \quad (5)$$

where the speed,  $v$ , of the H atom is given by  $[2E_{\text{t}}^{\text{lab}}(\text{H})/m_{\text{H}}]^{1/2}$ . The simulated curves shown by the solid line in Fig. 2 are in good agreement with the results. In this calculation, we assumed a Gaussian distribution for the total translational energy  $E_{\text{t}}$ , that is

$$P(E_{\text{t}}) = A \exp\left[-2.77 \frac{(E_{\text{t}} - \langle E_{\text{t}}(\text{H} + \text{HO}_2) \rangle)^2}{\sigma_{\text{t}}^2}\right], \quad (6)$$

where  $A$  is a normalization constant, and  $\sigma_{\text{t}}$  is the full-width-at-half-maximum of the distribution. The value of  $\sigma_{\text{t}}$  is treated as a fitting parameter, which corresponds to the internal energy distribution of the  $\text{HO}_2(\tilde{\text{X}})$  fragment. The best-fit value of  $\sigma_{\text{t}}$  is  $38 \text{ kJ mol}^{-1}$ .

When the dissociation lifetime of the photoexcited state is shorter than the rotational period of the parent molecule, the value of the anisotropy parameter,  $\beta$ , is given by,

$$\beta = 3 \cos^2 \chi - 1, \quad (7)$$

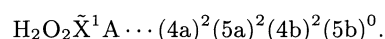
where  $\chi$  is the angle between the directions of the electronic transition moment and the dissociating bond. However, the parent molecular rotation reduces the anisotropy by a factor,  $f$ , which can be approximated for a small deflection of the original velocity vector<sup>13)</sup>

$$f = 1 - 3RT/(2)^{1/2} E_{\text{rel}}, \quad (8)$$

where  $E_{\text{rel}}$  is the recoil energy of the H and  $\text{HO}_2$  fragments. Since  $E_{\text{rel}}$  is  $149 \text{ kJ mol}^{-1}$ ,  $f$  is 0.97. The corrected value for the anisotropy parameter is given by  $\beta = \beta_{\text{eff}}/f$ , and is  $-0.24 \pm 0.10$ . This  $\beta$  value should be corrected for the incomplete polarization of the excimer laser light according to Dzvonik et al.<sup>14)</sup> The corrected anisotropy parameter,  $\beta$ , is  $-0.26 \pm 0.11$ .

## Discussion

The main configuration of the electronic ground state,  $\text{H}_2\text{O}_2(\tilde{\text{X}}^1\text{A})$ , at the equilibrium geometry is represented by



The last four molecular orbitals are denoted as  $\sigma_{\text{O}-\text{O}}$ ,  $n(\text{synphase})$ ,  $n(\text{antiphase})$ , and  $\sigma_{\text{O}-\text{O}}^*$ , respectively.<sup>1,2)</sup> The first absorption band is assigned to the transition from the ground state to the  $\tilde{\text{A}}^1\text{A}$  and  $\tilde{\text{B}}^1\text{B}$  states that are strongly repulsive on the O-O bond. It occurs from the highest occupied 4b level to the lowest unoccupied 5b level. The second transition is of  $(n, 3s)$ , which appears in the vacuum UV region. It occurs from the highest occupied 4b level to the unoccupied 6a level, i. e. the first s Rydberg orbital. Due to its Rydberg nature, this state must be like the first ion  $1^2\text{B}$  state and it must not itself be dissociative.

At 266 nm, Gericke et al.<sup>4)</sup> found a negative value of  $\beta = -0.72 \pm 0.10$  for the fragmentation to  $\text{OH} + \text{OH}$  from  $\text{H}_2\text{O}_2(\tilde{\text{A}}^1\text{A})$ , which indicates an upper limit for the molecular lifetime of 60 ps of  $\text{H}_2\text{O}_2(\tilde{\text{A}}^1\text{A})$ . At 248 nm, Docker et al.<sup>9)</sup> measured the OH fragment translational anisotropy by Doppler spectroscopy, identifying the dissociative state as the  $^1\text{A}$  state. Since the translational anisotropy is high, and  $\beta$  being close to its limiting value of  $-1$ , these results indicate an instantaneous dissociation of  $\text{H}_2\text{O}_2(\tilde{\text{A}}^1\text{A})$ . At 193 nm, Grunewald et al.<sup>15)</sup>

measured the vector correlations between the transition dipole moment of the parent  $\text{H}_2\text{O}_2$  and the OH product rotational motions by the Doppler broadened spectral lines, and found that  $\beta$  is  $-0.10$ . The quantitative contribution of the two different electronic excited states in the dissociation process was determined by analyzing the vector properties of the OH fragment. 62% of the OH products evolve from the  $\tilde{\text{A}}^1\text{A}$  electronic excited state, while 38% of the fragments are formed via the  $\tilde{\text{B}}^1\text{B}$  state when  $\text{H}_2\text{O}_2$  excited at 193 nm dissociates instantaneously into OH+OH.

A rationale for the observed angular distribution of the H atoms following excitation into the first continuum at 193 nm can be developed by considering the correlation diagrams and contours of the calculated potential energy surfaces. Figure 1 summarizes the important correlations and potential energy contours for the lower-lying electronic states. The first continuum is associated with both the  $\tilde{\text{A}}^1\text{A}$  and  $\tilde{\text{B}}^1\text{B}$  states, which are expected to be planar and nonplanar, respectively. In the planar configuration ( $C_{2h}$ ), the  $\tilde{\text{A}}^1\text{A}$  symmetry becomes  $^1\text{A}_g$ , which correlates with  $\text{H}(^2\text{S})+\text{HO}_2(\tilde{\text{X}}^2\text{A}'')$ ; the  $^1\text{B}$  symmetry, however, becomes  $^1\text{B}_u$ , which does not correlate with  $\text{H}(^2\text{S})+\text{HO}_2(\tilde{\text{X}}^2\text{A}'')$ .<sup>16)</sup> Thus, the main feature of this schematic potential energy surface for the  $\tilde{\text{A}}^1\text{A}$  state is a direct dissociation to  $\text{H}(^2\text{S})+\text{HO}_2(\tilde{\text{X}}^2\text{A}'')$ .

If the  $\tilde{\text{A}}^1\text{A}$  state is exclusively responsible for the H atom formation process at 193 nm and the transition moment,  $\mu$ , lies along the  $C_2$  axis, one should obtain a  $\beta$  value of  $-0.27$  for the H photofragment. In this calculation we assume that the bending angle,  $\angle\text{HOO}$ , is  $99.3^\circ$ , the torsional angle,  $\tau$ , is  $120.2^\circ$ , and the existence of an instantaneous dissociation.<sup>2)</sup> Ab initio calculations by Cheveldonnet et al.<sup>1)</sup> show that since the  $\tilde{\text{B}}^1\text{B}$  state is reached by a  $(\sigma_{\text{O}-\text{O}}, \sigma_{\text{O}-\text{O}}^*)$  or  $(5b) \leftarrow (4b)$  transition, the transition moment,  $\mu$ , is aligned essentially parallel to the O-O bond. According to their calculation, the angle between the internuclear axis and  $\mu$  is  $20^\circ$ . The expected anisotropy parameter for the H atom is given by  $\beta = -0.41$  for an instantaneous dissociation from the  $\tilde{\text{B}}^1\text{B}$  state. The observed anisotropy parameter ( $\beta = -0.26 \pm 0.11$ ) can be explained by exclusive formation from the  $\tilde{\text{A}}^1\text{A}$  state. When the  $\tilde{\text{B}}^1\text{B}$  state is reached, the H atom formation is small and the OH formation is dominant, since the  $\tilde{\text{B}}^1\text{B}$  state is not correlated adiabatically with the H atom formation process (Fig. 1) and dissociates instantaneously into OH+OH.

The result obtained for the kinetic energy release indicates that 60% of the available energy goes into the kinetic energy in the photodissociation of  $\text{H}_2\text{O}_2$  ( $\tilde{\text{A}}^1\text{A}$ ) at 193 nm to  $\text{H}(^2\text{S})+\text{HO}_2(\tilde{\text{X}}^2\text{A}'')$  and that excitation in the internal degree of freedom of the  $\text{HO}_2$  fragment is not very large. We can discuss the vibrational energy disposal in terms of Franck-Condon-excitation effects.<sup>17)</sup> The equilibrium molecular structure of the  $\text{H}_2\text{O}_2(\tilde{\text{X}}^1\text{A})$  molecule involves the internuclear distance  $R(\text{O}-\text{H})=0.967 \text{ \AA}$ ,  $R(\text{O}-\text{O})=1.463 \text{ \AA}$ , and a bending

angle  $99.3^\circ$ ,<sup>2)</sup> while that of the  $\text{HO}_2(\tilde{\text{X}}^2\text{A}'')$  radical is  $R(\text{O}-\text{H})=0.977 \text{ \AA}$ ,  $R(\text{O}-\text{O})=1.33 \text{ \AA}$ , and  $104^\circ$ .<sup>18)</sup> These structures are not very much different from each other. Therefore, according to the Franck-Condon principle, the vibrational excitation is expected to be small in the photodissociation of  $\text{H}_2\text{O}_2$  to  $\text{H}+\text{HO}_2$ . Furthermore, the orbital angular momentum produced by the O-H bond breaking in the photodissociation of  $\text{H}_2\text{O}_2$  is carried away by the H atom fragment, since the mass of H is much smaller than that of the O atom. This indicates that high rotational and vibrational excitations in the  $\text{HO}_2$  fragment may not occur in the photodissociation of  $\text{H}_2\text{O}_2$ . Thus, a fairly large amount of the available energy goes into the kinetic energy.

Thanks are due to Dr. K. Tonokura for his aid in the experiment and Mr. N. Kuroda for his technical assistance. This work is supported by the Grant-in-Aid from the Ministry of Education, Science and Culture.

## References

- 1) C. Cheveldonnet, H. Cady, and A. Dargelos, *Chem. Phys.*, **102**, 55 (1986).
- 2) A. Morita and S. Kato, *J. Phys. Chem.*, **96**, 1067 (1992).
- 3) C. L. Lin, N. K. Rohatgi, and W. B. DeMore, *Geophys. Res. Lett.*, **5**, 113 (1978).
- 4) K.-H. Gericke, S. Klee, F. J. Comes, and R. N. Dixon, *J. Chem. Phys.*, **85**, 4463 (1986); K.-H. Gericke, *Faraday Discuss. Chem. Soc.*, **82**, 41 (1986).
- 5) M. B. Robin, "Higher Excited States of Polyatomic Molecules," Academic Press, Orlando (1985).
- 6) U. Gerlach-Meyer, E. Linnebach, K. Kleinermanns, and J. Wolfrum, *Chem. Phys. Lett.*, **133**, 113 (1987).
- 7) G. L. Vaghjiani and A. R. Ravishankara, *J. Chem. Phys.*, **92**, 996 (1990); G. L. Vaghjiani, A. A. Turnispeed, R. F. Warren, and A. R. Ravishankara, *J. Chem. Phys.*, **96**, 5878 (1992).
- 8) L. J. Stief and V. J. De Carlo, *J. Chem. Phys.*, **50**, 1234 (1969).
- 9) M. P. Docker, A. Hodgson, and J. P. Simons, *Faraday Discuss. Chem. Soc.*, **82**, 25 (1986); R. Schinke, *J. Phys. Chem.*, **92**, 4015 (1988).
- 10) G. Hilbig, A. Lago, and R. J. Wallenstein, *J. Opt. Soc. Am.*, **1987**, B4, 1753.
- 11) R. N. Zare and D. R. Herschbach, *Proc. IEEE*, **51**, 173 (1963).
- 12) H. L. Kim, S. Satyapal, P. Brewer, and R. Bersohn, *J. Chem. Phys.*, **91**, 1047 (1989).
- 13) S.-C. Yang and R. Bersohn, *J. Chem. Phys.*, **61**, 4400 (1971).
- 14) M. Dzvonik, S.-C. Yang, and R. Bersohn, *J. Chem. Phys.*, **61**, 4410 (1972).
- 15) A. V. Grunewald, K.-H. Gericke, and F. J. Comes, *J. Chem. Phys.*, **87**, 5709 (1987).
- 16) G. Herzberg, "Molecular Spectra and Molecular Structure," Van Nostrand Reinhold Co., New York (1966), Vol. 3, Tables 27, 28.
- 17) R. C. Mitchell and J. P. Simons, *Discuss. Faraday*

*Soc.*, **44**, 208 (1967).

18) Y. Beers and C. J. Howard, *J. Chem. Phys.*, **64**, 1541 (1976).

---